Secondary Structure and Gating Rearrangements of Transmembrane Segments in Rat $P2X_4$ Receptor Channels

Shai D. Silberberg, Tsg-Hui Chang, and Kenton J. Swartz

Molecular Physiology and Biophysics Section, Porter Neuroscience Research Center, National Institute of Neurological Disorders and Stroke, National Institutes of Health, Bethesda, MD 20892

ABSTRACT P2X receptors are cation selective channels that are activated by extracellular nucleotides. These channels are likely formed by three identical or related subunits, each having two transmembrane segments (TM1 and TM2). To identify regions that undergo rearrangement during gating and to probe their secondary structure, we performed tryptophan scanning mutagenesis on the two putative TMs of the rat $P2X_4$ receptor channel. Mutant channels were expressed in *Xenopus* oocytes, concentration–response relationships constructed for ATP, and the EC_{50} estimated by fitting the Hill equation to the data. Of the 22 mutations in TM1 and 24 in TM2, all but one in TM1 and seven in TM2 result in functional channels. Interestingly, the majority of the functional mutants display an increased sensitivity to ATP, and in general these perturbations are more pronounced for TM2 when compared with TM1. For TM1 and for the outer half of TM2, the perturbations are consistent with these regions adopting α-helical secondary structures. In addition, the greatest perturbations in the gating equilibrium occur for mutations near the outer ends of both TM1 and TM2. Surface biotinylation experiments reveal that all the nonfunctional mutants traffic to the surface membrane at levels comparable to the WT channel, suggesting that these mutations likely disrupt ion conduction or gating. Taken together, these results suggest that the outer parts of TM1 and TM2 are helical and that they move during activation. The observation that the majority of nonconducting mutations are clustered toward the inner end of TM2 suggests a critical functional role for this region.

KEY WORDS: purinergic receptors • point mutation • scanning mutagenesis • oocytes • ligand-gated channel

The Journal of General Physiology

INTRODUCTION

P2X receptors are cation channels that are gated by extracellular nucleotides. These widely distributed ion channels are highly permeable to calcium (Egan and Khakh, 2004), and perform diverse physiological functions (for a comprehensive recent review see North, 2002). Over the past decade, seven mammalian P2X receptor subunits have been cloned ($P2X_1$–$P2X_7$) that form both homomeric and heteromeric channel assemblies (Brake et al., 1994; Valera et al., 1994; North, 2002). P2X receptor channels have structural and functional properties distinct from other ligand-gated channels. They are likely formed by three identical or related subunits (Nicke et al., 1998; Stoop et al., 1999; Jiang et al., 2003a; Aschrafi et al., 2004), each having a large extracellular segment of ~280 amino acids that is flanked by two transmembrane segments (TM1 and TM2), placing both the NH_2 and COOH termini intracellular (Newbolt et al., 1998) (Fig. 1 A). In contrast, ion channels of the Cys-loop family (e.g., nicotinic acetylcholine receptor channels) contain five subunits, with each subunit having four transmembrane segments (Lester et al., 2004), whereas glutamate gated ion channels are tetramers in which each subunit has three segments that cross the membrane (Wollmuth and Sobolevsky, 2004). P2X receptor channels are also distinct in the ability to produce a large conductance pathway. Cells expressing homomeric $P2X_2$, $P2X_4$, or $P2X_7$ receptor channels, as well as $P2X_{2/3}$ heteromeric receptor channels, become permeable to molecules as large as YO-PRO-1 dye (523 D for the free cation) following long exposures to extracellular ATP, suggesting that the channels undergo pore dilation (Khakh et al., 1999; Virginio et al., 1999). The molecular mechanism for the increase in permeability is still not known, nor is it clear how the TMs are arranged around the pore.

In most channels of known structure, the membrane-spanning segments adopt α-helical secondary structures (Walz et al., 1997; Chang et al., 1998; Doyle et al., 1998; Dutzler et al., 2002; Jiang et al., 2002b, 2003b; Kuo et al., 2003; Miyazawa et al., 2003). However, scanning cysteine accessibility experiments on the two TMs of rat $P2X_2$ receptor channels did not resolve their secondary structure. Using methanethiosulfonate (MTS) reagents on TM2, Rassendren et al. (1997) concluded that their results do not support the hypothesis that the pore is

Correspondence to Shai D. Silberberg: silberbs@ninds.nih.gov

S.D. Silberberg's permanent address is Department of Life Sciences, Ben-Gurion University of the Negev, P.O. Box 653, Beer-Sheva 84105, Israel.

Abbreviations used in this paper: MTS, methanethiosulfonate; TM, transmembrane; WT, wild-type.

http://www.jgp.org/cgi/doi/10.1085/jgp.200409221

formed as the polar face of an amphipathic helix. A separate MTS and silver accessibility study on TM2 of the $P2X_2$ receptor channel discusses the secondary structure of the TM but seems to argue against helical structure (Egan et al., 1998). Two studies were performed on TM1, both of which make no assessment of helical structure (Haines et al., 2001b; Jiang et al., 2001).

An alternate approach to examining secondary structure is alanine or tryptophan scanning mutagenesis. The rationale behind this approach has been previously discussed (Monks et al., 1999; Li-Smerin et al., 2000a). The underlying assumption is that side chains exposed to the lipid membrane in both closed and open conformations would be relatively tolerant to mutation, as long as the substituted amino acid is hydrophobic. In contrast, side chains involved in protein packing in either closed or open conformations would be relatively sensitive to mutation. For an α-helix with a significant lipid-exposed surface, a pattern might emerge in which every third or forth residue exhibits a similar sensitivity to the mutation. This approach has been used successfully for inward rectifier potassium channels (Choe et al., 1995; Cukras et al., 2002), voltage-activated potassium channels (Monks et al., 1999; Hong and Miller, 2000; Li-Smerin et al., 2000a,b; Li-Smerin and Swartz, 2001; Hackos et al., 2002), nicotinic acetylcholine receptor channels (Tamamizu et al., 2000; Guzman et al., 2003), glutamate receptor channels (Panchenko et al., 2001), and $GABA_A$ receptor channels (Jenkins et al., 2002). More recently, while the present manuscript was in writing, an alanine scan of both TMs in $P2X_2$ was published (Li et al., 2004). This alanine scan is consistent with helical structure for TM1 and is inconclusive for TM2.

In the present study, we used scanning mutagenesis on the rat $P2X_4$ receptor channel to probe the secondary structure of the TMs and to identify regions that undergo rearrangements during gating. We individually replaced each residue in the two TMs with tryptophan, and in one case mutated a tryptophan to alanine, expressed each mutant channel in oocytes, and then examined the concentration dependence for activation of the channel by ATP. The results have important implications for the structure of P2X receptor channels and for the movements of the TMs during gating. A preliminary report of some of these observations has appeared (Silberberg and Swartz, 2004).

MATERIALS AND METHODS

Mutagenesis

Rat $P2X_4$ cDNA in pcDNA3 (provided by F. Soto, Max-Planck Institute for Experimental Medicine, Göettingen, Germany) was subcloned into pGEM-HE vector (Liman et al., 1992) in order to improve expression in oocytes. Mutant P2X receptor channels were generated by PCR using the $P2X_4$ DNA as template. The generation of the various mutations was confirmed by DNA sequencing. Mutant and wild-type (WT) P2X receptor channel cRNA was synthesized using T7 polymerase from DNA linearized with NotI.

Electrophysiological Recording

The WT and mutant channels were expressed in *Xenopus* oocytes by injecting ~50 nl of cRNA per oocyte at different dilutions. Membrane currents were recorded under voltage clamp using an OC-725C oocytes clamp amplifier (Warner Instrument Corp.) and digitized online using a Digidata 1321A interface board and pCLAMP 9 software (Axon Instruments). The sampling frequency was set to at least two times the corner frequency of the low-pass filter. To minimize voltage-clamp errors, the maximal current recorded from each mutant was limited by adjusting the amount of cRNA injected, by the time between cRNA injection and current recording, and by the holding voltage during current recording. The recording solution contained (in mM): 100 NaCl, 5 Hepes, 1 $MgCl_2$, 0.3 $CaCl_2$, pH 7.6. Solutions containing ATP were prepared freshly each day and the pH of the solution was readjusted.

Concentration–response relationships were constructed for the WT channel and for each of the mutant channels. In the early experiments, each tested concentration of ATP was bracketed by a measurement with a reference concentration of ATP. The currents were then corrected for desensitization by normalizing the current activated by a given concentration of ATP to the current activated by the preceding reference concentration of ATP. At least four individual concentration–response relationships were then averaged. In most experiments, however, each oocyte was used to test a single concentration of ATP. A reference concentration of ATP was applied first, followed 2 min later by a test concentration. Responses to the test concentrations of ATP were then normalized to the reference concentration. Each concentration was tested on at least four oocytes and all oocytes used to generate a concentration–response relationship were from the same batch.

Analysis

The Hill equation was fit to concentration-response relationships using SigmaPlot 2000 software (SPSS Inc.) according to

$$\frac{I}{I_{max}} = \frac{[ATP]^n}{[ATP]^n + EC_{50}{}^n},$$

where I is the normalized current at a given concentration of ATP, I_{max} is the maximum normalized current, EC_{50} is the concentration of ATP ([ATP]) yielding a current half the maximum, and n is the Hill coefficient. The results are reported as the mean ± SEM where SEM represents the goodness of fit of the Hill equation.

Fourier transform methods (Cornette et al., 1987; Komiya et al., 1988; Rees et al., 1989a,b; Li-Smerin et al., 2000a; Li-Smerin and Swartz, 2001) were used to evaluate the periodicity of the perturbations in EC_{50} for mutations in various regions of TM1 according to

$$P(\omega) = [X(\omega)^2 + Y(\omega)^2],$$

where

$$X(\omega) = \sum_{i=1}^{n} [(E_i - \bar{E})\sin(i\omega)]$$

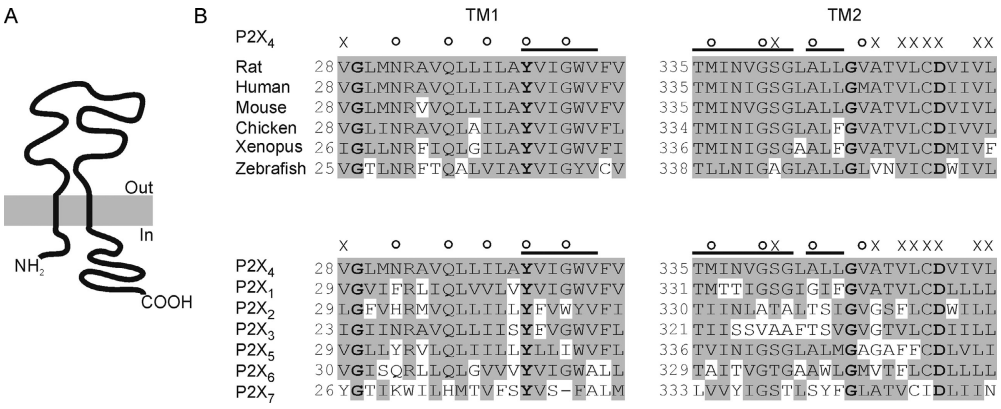

FIGURE 1. Putative transmembrane regions of P2X receptor channels. (A) Schematic representation of the general topology of a P2X receptor channel subunit. (B) Sequence alignment of TM1 (left) and TM2 (right) of $P2X_4$ receptor channels from different species (top) and of rat $P2X_1$–$P2X_7$ (bottom). Bold residues are identical across all known P2X receptor channels (except for a Y to F substitution in *Xenopus* $P2X_7$). The major findings of this study are summarized above the sequences. X indicates mutations to tryptophan that result in nonconducting channels. Empty circles and bars indicate positions and regions of large perturbations in EC_{50} induced by the mutations, respectively.

and

$$Y(\omega) = \sum_{i=1}^{n} [(E_i - \bar{E})\cos(i\omega)]$$

$P(\omega)$ is the Fourier transform power spectrum as a function of the angle between adjacent side chains (ω), n is the number of residues of a segment, E_i is the fold change in EC_{50} relative to WT at a given position i, and $\bar{E}$ is the average value of the fold change in EC_{50} for the segment.

The ratio of the mean power in the range of 100 ± 15° over the mean power of the entire spectrum (α-PI) was calculated to quantitatively evaluate the α-helical character from power spectra according to

$$\alpha\text{-PI} = \left[1/30 \int_{85^0}^{115^0} P(\omega)d\omega\right] \Big/ \left[1/180 \int_{0^0}^{180^0} P(\omega)d\omega\right].$$

Values of α-PI > 2 have been considered indicative of α-helical secondary structure (Cornette et al., 1987; Rees et al., 1989b).

Detection of Surface Protein

Surface protein was detected using the procedure of Ennion and Evans (2002) with slight modifications. 3 d after injection of cRNA, oocytes were incubated for 30 min at room temperature with Sulfo-NHS-LC-Biotin (0.5 mg/ml; Pierce Chemical Co.) in ND96 buffer containing (in mM) 96 NaCl, 2 KCl, 1.8 $CaCl_2$, 1 $MgCl_2$, 5 Na-Hepes, pH 7.6. After washing six times in ND96 buffer, oocytes were homogenized in 400 μl of buffer H containing (in mM) 100 NaCl, 20 Tris.Cl, pH 7.4, 1% Triton X-100, 5 μl/ml protease inhibitor cocktail (EMD Bioscience). Homogenization and all subsequent steps were performed at 4°C. After centrifugation at 16,000 *g* for 2 min, a 20-μl aliquot of the supernatant (total protein) was mixed with equal volume of 2× LDS sample buffer plus reducing agent: 50% 4× LDS sample buffer (Invitrogen), 20% 2-mercaptoethanol, 100 mM DTT. The remaining supernatant was diluted 1:1 with buffer H plus 50 μl of streptavidin agarose beads (Pierce Chemical Co.) and then tumbled gently overnight at 4°C. The streptavidin agarose beads were washed six times with buffer H with a 2-min centrifugation (16,000 *g*) between each wash. At the end of the final wash, 40 μl of 1× LDS sample buffer plus reducing agent was added to the beads and samples were heated at 95°C for 10 min. Following a 2-min centrifugation (16,000 *g*), the supernatant (surface protein) and total protein (collected earlier) were separated in a 4–12% Nu-Page Bis-Tris gel (Invitrogen) using a running buffer containing (in mM) 50 MOPS, 50 Tris base, 3.46 SDS, and 1 EDTA. See-Blue-Plus2 (Invitrogen) was used as the protein molecular weight marker. Protein in the gel was transferred to nitrocellulose membrane (Amersham Biosciences) where the transfer buffer contained (in mM) 25 bicine, 25 bis-tris, 1 EDTA, and 20% methanol. The nitrocellulose membrane was probed with rabbit anti-$P2X_4$ antibody (Alomone Labs) diluted 1:400 in PBS-T containing (in mM) 137 NaCl, 2.7 KCl, 10 Na_2HPO_4, 2 KH_2PO_4, 0.05% Tween-20, and $P2X_4$ expression was detected using ECL Western blotting detection reagents (Amersham Biosciences). The mutant *Shaker* potassium channels used as a control lacked residues 6–46 and contained c-myc epitopes inserted at both termini (for details see Hackos et al., 2002). For the Shaker Kv gels, the nitrocellulose membrane was probed with anti-myc antibody (Invitrogen).

RESULTS

The objective of this study was to use tryptophan scanning mutagenesis to probe the secondary structure of the TMs in P2X receptor channels and to identify regions that undergo rearrangement during gating. Fig. 1 B shows the regions of the rat $P2X_4$ receptor channel that were mutated, aligned either with $P2X_4$ receptor channel subunits cloned from other species (top), or with the other cloned rat P2X receptor subunits (bottom). Each residue was individually mutated to tryptophan, except for W46, which was mutated to alanine. Following expression in *Xenopus* oocytes, two-electrode voltage clamp techniques were used to measure ATP-activated membrane currents and construct concentration–response relationships for each mutant channel. For most mutations, each oocyte was used to test a single concentration of ATP in order to circumvent potential errors in the concentration–response relationship arising from incomplete recovery from desensitization between applications of ATP. A reference concentration of ATP was applied first, followed 2 min later by a test concentration (Fig. 2 A). Responses to the test concentrations of ATP were then normalized to the reference concentration. Superimposed normalized current

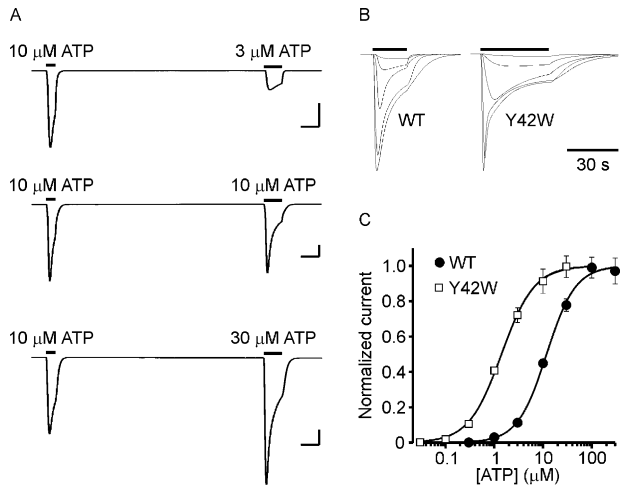

FIGURE 2. Generation of concentration–response relationships. (A) Representative current traces in response to ATP recorded from oocytes expressing WT $P2X_4$ receptor channels. Each trace is from a different oocyte. A reference concentration of ATP (3 μM) was applied first followed 2 min later by a test concentration (indicated by solid bars above the current traces). Calibration bars: 10 s and 0.2 μA. (B) Superimposed normalized current traces of WT (left) and Y42W (right) receptor channels. The bars above the current traces indicate the duration of ATP application. The concentrations of ATP are 1.0, 3.0, 10, 30, and 100 μM for WT and 0.1, 0.3, 1.0, 3.0, and 10 μM for Y42W. (C) Normalized concentration–response relationships for the WT receptor channel (full circles) and for Y42W (empty squares). Each point is the average ± SEM of 4–5 measurements. The EC_{50} and (n) estimated from fitting the Hill equation to the WT and Y42W data are 11.8 ± 0.7 μM, (1.5 ± 0.1), and 1.4 ± 0.1 μM, (1.3 ± 0.1), respectively.

TABLE I

Estimated EC_{50} and n for the Mutations in TM1

Mutation	EC_{50} (μM)	n	Fold change in EC_{50}[a]
WT	11.8 ± 0.7	1.5 ± 0.1	1.0
V49W	8.2 ± 1.9	1.3 ± 0.3	1.4
F48W	5.5 ± 0.2	1.5 ± 0.1	2.2
V47W	1.4 ± 0.3	1.0 ± 0.2	8.4
W46A	2.0 ± 0.1	1.6 ± 0.1	5.9
G45W	0.5 ± 0.04	1.4 ± 0.1	23.6
I44W	1.5 ± 0.1	1.9 ± 0.3	7.9
V43W	1.6 ± 0.2	1.3 ± 0.1	7.4
Y42W	1.4 ± 0.1	1.3 ± 0.1	8.4
A41W	11.3 ± 0.2	1.6 ± 0.05	1.0
L40W	>30	ND[b]	<0.4
I39W	2.0 ± 0.2	1.4 ± 0.1	5.9
L38W	7.6 ± 0.6	1.2 ± 0.1	1.6
L37W	13.5 ± 0.7	1.4 ± 0.1	0.9
Q36W	2.7 ± 0.1	1.6 ± 0.1	4.4
V35W	14.5 ± 3.5	1.1 ± 0.1	0.8
A34W	8.7 ± 0.9	1.2 ± 0.1	1.4
R33W	6.1 ± 0.4	1.4 ± 0.1	1.9
N32W	2.9 ± 0.2	1.4 ± 0.1	4.1
M31W	6.1 ± 1.3	1.0 ± 0.1	1.9
L30W	12.2 ± 1.6	1.0 ± 0.1	1.0
G29W	9.1 ± 0.8	1.2 ± 0.1	1.3
V28W	ND	ND	

[a]Fold change in EC_{50} was calculated as EC_{50}(WT)/EC_{50}(mutant).
[b]ND, not determined.

traces, activated by a range of ATP concentrations, for the WT receptor channel and for Y42W are shown in Fig. 2 B. The mean (±SEM) normalized current for a range of ATP concentrations are plotted in Fig. 2 C for the WT channel (black circles) and for Y42W (white squares). A Hill equation was fit to the data (solid lines through the data in Fig. 2 C), giving an EC_{50} and (n) of 11.8 ± 0.7 μM and (1.5 ± 0.1), and 1.4 ± 0.1 μM and (1.3 ± 0.1), for the WT and Y42W receptor channels, respectively. This analysis reveals that the Y42W mutant channel is significantly more sensitive to ATP when compared with the WT channel.

Tryptophan Scanning TM1

Of the 22 mutants studied in TM1, all except V28W give rise to ATP-gated currents when expressed in *Xenopus* oocytes. Concentration–response relationships can readily be constructed for all of the conducting mutants aside from L40W, which requires several minutes to fully deactivate following the application of ATP. Table I summarizes the estimated EC_{50} and n for the mutations in TM1. Because changes in n are not easily interpretable and since no obvious trend in n is observed, we focus on the estimated EC_{50} values, which are presented in a histogram in Fig. 3 A. The vertical solid and dashed lines represent the EC_{50} ± SEM of the WT receptor channel. Although the sensitivity of some mutants to ATP is similar to the WT channel, it is immediately apparent that many of the mutant channels display a perturbed sensitivity to ATP. Remarkably, with only one exception (L40W, see Table I), these latter mutants all display an increased sensitivity to ATP, as seen by a leftward shift in EC_{50}. It is unlikely that these mutations enhance ATP binding affinity directly because the ATP binding pocket is thought to reside elsewhere (Nakazawa et al., 1998a; Ennion et al., 2000; Jiang et al., 2000; Roberts and Evans, 2004), and it is unlikely that so many residues would directly contribute to the agonist binding site for such a small ligand. ATP binding promotes opening of the gate in P2X receptors, and thus the leftward perturbations in EC_{50} probably reflect changes in the relative stability of the open and closed conformations. By shifting this equilibrium toward the open state, the mutations in TM1 bias the ATP binding step toward the bound state. The interesting observation that so many mutations shift the close–open equilibrium toward the open state will be addressed further in DISCUSSION.

Visual examination of the perturbations in EC_{50} (Fig. 3 A) reveals that for every third or forth residue (N32W,

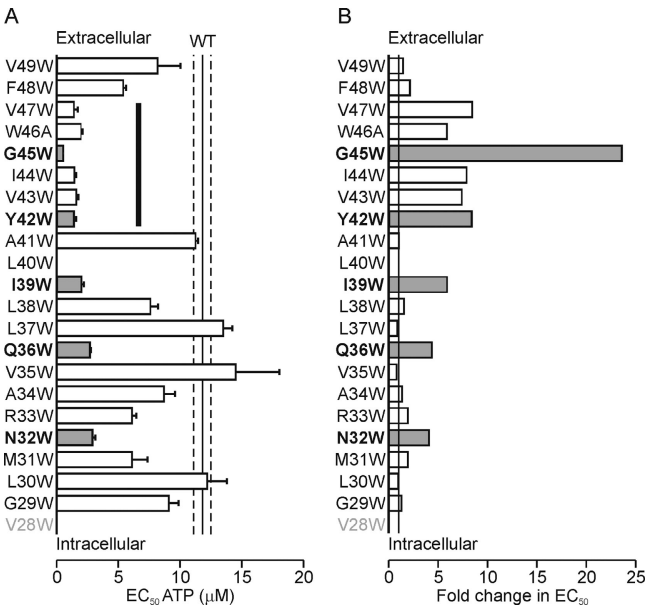

FIGURE 3. Tryptophan substitution at many positions in TM1 increases sensitivity to ATP. Estimated EC_{50} ± SEM (A) and fold changes in EC_{50} relative to WT (B) for each of the point mutations in TM1. Only V28W does not give rise to measurable currents. A concentration–response relationship could not be generated for L40W. The mean ± SEM of the EC_{50} for WT receptor channels is represented by a vertical line and vertical dashed lines, respectively. Every third or fourth residue exhibits a greater perturbation in EC_{50} relative to its neighboring residues (bold typeface, full bars). Toward the outer region of TM1 there are six successive mutations with large perturbations in EC_{50} (vertical bar in A).

Q36W, I39W, Y42W, and G45W; bold typeface and shaded bars) the perturbation in EC_{50} is greater than those of the neighboring residues. This is more clearly seen when the fold change in EC_{50} relative to WT is examined (Fig. 3 B). For these "high impact" positions, the magnitude of the perturbation progressively increases from inside to outside. When mapped onto a helical projection of TM1, the five residues labeled in Fig. 3 are located on one side of the wheel, pointing to a face of an α-helix that is likely to be involved in protein–protein interactions (Fig. 4 A). Mapping these residues on a helical net diagram of TM1 shows that the sensitive face of TM1 spans most of the length of the segment (Fig. 4 B). To quantify the observed pattern in TM1, we used Fourier analysis, which can identify periodicity in the data (see MATERIALS AND METHODS). The periodicity for an α-helix residing in a bimodal environment (e.g., an amphipathic helix) is ~100° (360°/3.6 residues per turn). For the region between G29W and V43W, the strongest peak in the power spectrum of the fold change in EC_{50} is observed at 102° and the calculated periodicity index (α-PI) is 2.3 (Fig. 4 C), suggesting that this region adopts an α-helical secondary structure. For longer segments of TM1, the power spectra are more complex, resulting from an increased ATP sensitivity observed for each consecutive position between Y42W and V47W (black bar in Fig. 3 A). However, the clear helical pattern in EC_{50} perturbations (Figs. 3 and 4) encompasses the entire length of TM1, suggesting that this entire segment is an α-helix.

Tryptophan Scanning TM2

In the region of the second TM, we mutated each residue between T335 and L358 to tryptophan (Fig. 1 B). Table II summarizes the estimated EC_{50} and n for the mutations in TM2, and the estimated EC_{50} values are also shown graphically in Fig. 5 A. The results for TM2 are clearly more complex than for TM1. 7 out of the

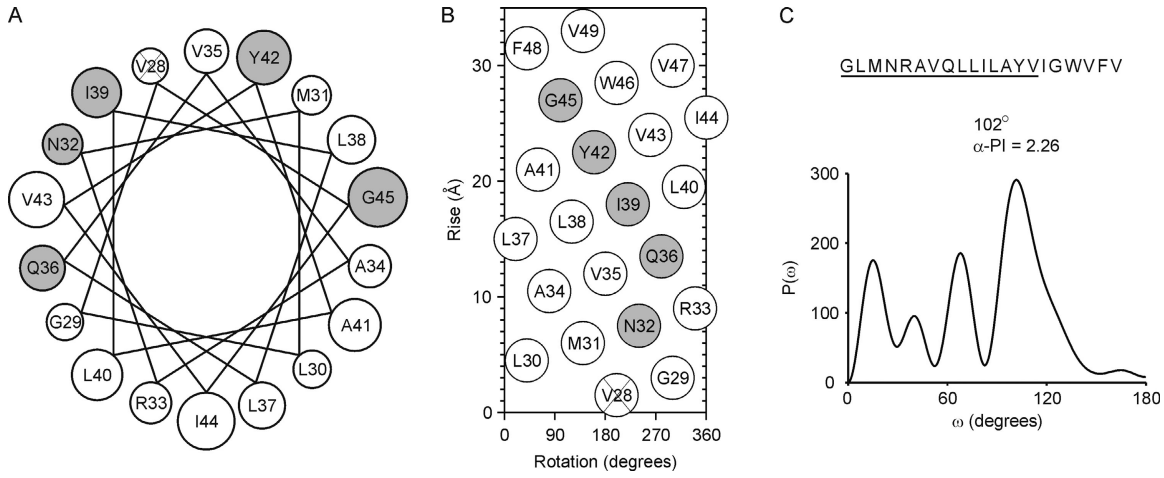

FIGURE 4. TM1 is likely an α-helix. Helical wheel representation (A) and helical net diagram (B) of TM1. The residues in the helical wheel representation progressively decrease in size from the outer to inner ends of TM1 (residues W46–V49 are not shown). The residues labeled in bold typeface in Fig. 3 map to one face of a presumed α-helix. (C) Fourier analysis of the fold change in EC_{50} for the region of TM1 underlined above. The primary peak of the power spectrum occurs at 102°. The α-PI calculated from the spectrum is 2.26. The EC_{50} for L40W was taken to be 30 μM (see Table I).

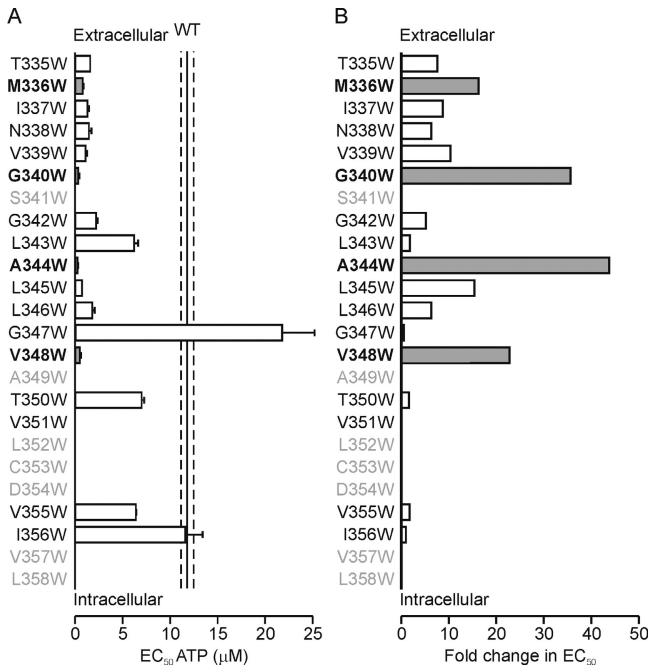

FIGURE 5. Tryptophan substitution increases sensitivity to ATP in many positions in TM2. Estimated EC_{50} ± SEM (A) and fold changes in EC_{50} relative to WT (B) for each of the point mutations in TM2. Seven residues, six of which are toward the inner region of TM2, do not give rise to measurable currents (light gray typeface). A concentration–response relationship could not be determined for V351W. The mean ± SEM EC_{50} for WT is represented by a vertical line and vertical dashed lines, respectively. Toward the outer region of TM2 the perturbations in EC_{50} are large and the four mutants with the greatest perturbations are four residues apart. (bold typeface, full bars).

TABLE II

Estimated EC_{50} and n for the Tryptophan Mutations in TM2

Mutation	EC_{50} (μM)	*n*	Fold change in EC_{50}[a]
WT	11.8 ± 0.7	1.5 ± 0.1	1.0
T335W	1.6 ± 0.01	2.0 ± 0.01	7.4
M336W	0.8 ± 0.1	1.2 ± 0.1	14.8
I337W	1.3 ± 0.1	1.4 ± 0.2	9.1
N338W	1.5 ± 0.3	1.4 ± 0.3	7.9
V339W	1.1 ± 0.1	2.2 ± 0.6	10.7
G340W	0.3 ± 0.1	0.9 ± 0.2	39.3
S341W	ND[b]	ND	
G342W	2.2 ± 0.2	1.7 ± 0.2	5.4
L343W	6.3 ± 0.4	1.4 ± 0.1	1.9
A344W	0.3 ± 0.06	1.0 ± 0.2	39.3
L345W	0.7 ± 0.01	1.8 ± 0.04	16.9
L346W	1.8 ± 0.3	1.3 ± 0.2	6.6
G347W	21.8 ± 3.4	1.1 ± 0.1	0.5
V348W	0.5 ± 0.1	1.2 ± 0.2	23.6
A349W	ND	ND	
T350W	7.0 ± 0.3	1.4 ± 0.04	1.7
V351W	ND	ND	
L352W	ND	ND	
C353W	ND	ND	
D354W	ND	ND	
V355W	6.4 ± 0.1	1.8 ± 0.01	1.8
I356W	11.6 ± 1.8	2.0 ± 0.6	1.0
V357W	ND	ND	
L358W	ND	ND	

[a]Fold change in EC_{50} was calculated as EC_{50}(WT)/EC_{50}(mutant).
[b]ND, not determined.

24 mutated residues (S341W, A349W, L352W, C353W, D354W, V357W, and L358W) located primarily toward the inside of TM2, do not give rise to ATP-gated currents (when exposed to 300 μM ATP), while three residues (N338W, G340W, and V351W) give small currents. A concentration–response relationship could not be constructed for V351W, which like L40W in TM1 requires several minutes to fully deactivate following the application of ATP. Aside from G347W and I356W, all of the remaining mutants are more sensitive to ATP relative to WT. Large perturbations in EC_{50} are observed toward the outside of TM2, similar to TM1, however, the magnitude of perturbations in TM2 is considerably greater than for TM1. In TM2, 5 out of 17 functional mutations result in a >10-fold increase in sensitivity to ATP, whereas in TM1, only 1 out of 21 functional mutants results in a similar change in sensitivity (see Tables I and II). Finally, for the outer half of TM2, the largest perturbations in EC_{50} are at every fourth position (M336W, G340W, A344W, and V348W; bold typeface and shaded bars), as most clearly seen when the fold change in EC_{50} relative to WT is plotted (Fig. 5 B).

Of the seven mutations that result in nonfunctional channels, six are located near the inner end of TM2, significantly restricting an examination of helical periodicity. However, for the outer half of TM2, the four mutations that cause the largest perturbations in EC_{50} are distributed in a helical pattern, mapping to one side of a helical wheel representation and lying on a single face of a helical net representation (Fig. 6). Fourier analysis was not performed on the limited data for TM2 since the longest uninterrupted region is seven residues long. Hence, while the pattern in ATP sensitivity suggests that the outer region of TM2 is an α-helix, the pattern is not as unambiguous as for TM1.

Trafficking of the Nonfunctional Mutants to the Surface Membrane

Although at many positions tryptophan substitution amounts to a rather radical mutation, the majority of mutants in this study (38 out of 46), and in previous tryptophan scanning mutagenesis studies (Collins et al., 1997; Monks et al., 1999; Hong and Miller, 2000; Li-Smerin et al., 2000a,b; Tamamizu et al., 2000; Panchenko et al., 2001; Hackos et al., 2002; Jenkins et al., 2002; Guzman et al., 2003), result in channels that

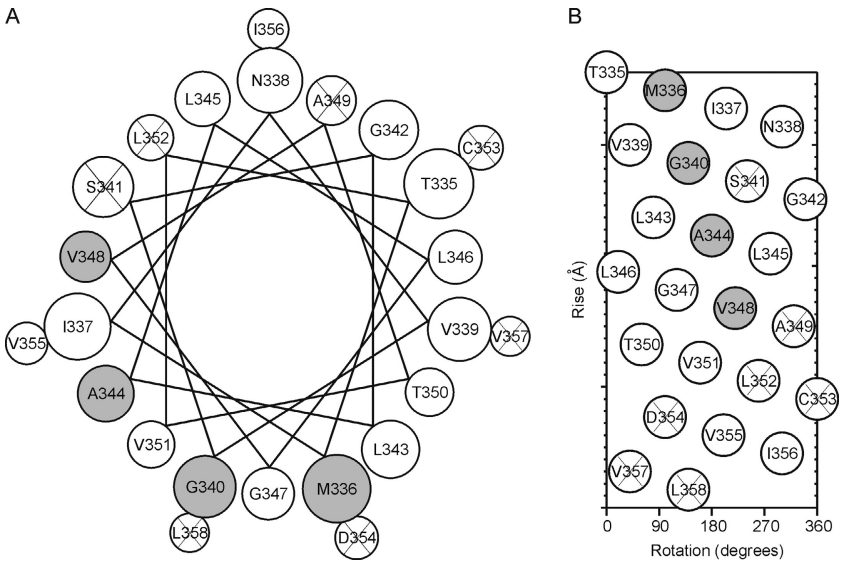

FIGURE 6. The extracellular region of TM2 seems to be an α-helix. Helical wheel representation (A) and helical net diagram (B) of TM2. The residues in the helical wheel representation progressively decrease in size from the outer to inner ends of TM2. The residues labeled in bold typeface in Fig. 5 map to one face of a presumed α-helix.

fold properly, traffic to the plasma membrane, and form functional channels. Do the eight mutations (one in TM1 and seven in TM2) that fail to give rise to membrane currents disrupt folding and/or trafficking, or are the native residues vital for channel function? To address this question, we estimated the surface protein expression level for each of the nonfunctional mutants and compared it to that of the WT channel.

To this end, oocytes were injected with equal amounts of cRNA encoding WT or mutant $P2X_4$ channels, and after 3 d to allow for expression, the surface membrane proteins of intact oocytes were biotinylated using a membrane-impermeant, primary amine–specific, biotinylation reagent. Biotinylated oocytes were then washed, homogenized, and centrifuged to isolate a crude protein fraction (see MATERIALS AND METHODS). A small aliquot of the crude fraction (equivalent to one oocyte) was used to evaluate the quantities of $P2X_4$ receptor channel protein in total oocyte membranes. The remaining membrane sample was purified using streptavidin agarose beads. Following PAGE separation (20 oocytes per lane), proteins were transferred to nitrocellulose membrane, probed with rabbit anti-$P2X_4$ antibody, and detected using ECL. We also estimated the amount of WT $P2X_4$ channel protein from oocytes that were not treated with the biotinylation reagent in order to evaluate the specificity of the streptavidin agarose bead fractionation for biotinylated protein. No $P2X_4$ receptor channel protein is detected in the bead fraction of nonbiotinylated oocytes (Fig. 7 A, top), confirming the specificity of the fractionation procedure. When the levels of $P2X_4$ protein in total and surface membranes are compared for the WT and nonfunctional mutants, a rather surprising result is seen: the protein levels in the surface membrane fractions for each of the nonfunctional mutants are indistinguishable from the WT $P2X_4$ receptor channel (Fig. 7 A, top).

To confirm that the biotinylation reagent selectively labels surface proteins, we performed parallel experiments with the *Shaker* Kv channels, where specific mutants have been documented to be retained in the ER. Two c-myc–tagged *Shaker* Kv channel mutants, a nonfunctional mutant that is retained in the ER (I477D), and a weakly conducting mutant with surface membrane expression comparable to the WT *Shaker* Kv channel (F481W), were expressed in oocytes and isolated in parallel with $P2X_4$ receptor channels. As previously reported (Hackos et al., 2002), two dominant forms of F481W are detected in the crude membrane preparation: a core-glycosylated species (~70 kD), corresponding to ER-retained protein, and a more heavily glycosylated form (~100 kD) that can traffic to the surface membrane. In contrast, for I477D, only the core-glycosylated species is observed in the crude membrane preparation (Fig. 7 B). If the biotinylated surface membrane fraction is contaminated with protein from internal membranes (in the unlikely event that biotin was to gain access into the oocytes), we would expect to observe both core-glycosylated *Shaker* protein and the heavily glycosylated form in the biotinylated fraction. However, for the mutant that traffics to the surface membrane (F481W), only the heavily glycosylated form is detected in the biotinylated surface membrane fraction, and for the ER-retained mutant (I477D), no *Shaker* protein is observed in this fraction (Fig. 7 B). These control experiments clearly demonstrate that the surface protein preparation is not contaminated by the intracellular membrane fraction. Taken together, these results suggest that all of the nonfunctional $P2X_4$ channel mutants fold properly and efficiently traffic to the surface membrane. This contrasts with nonfunc-

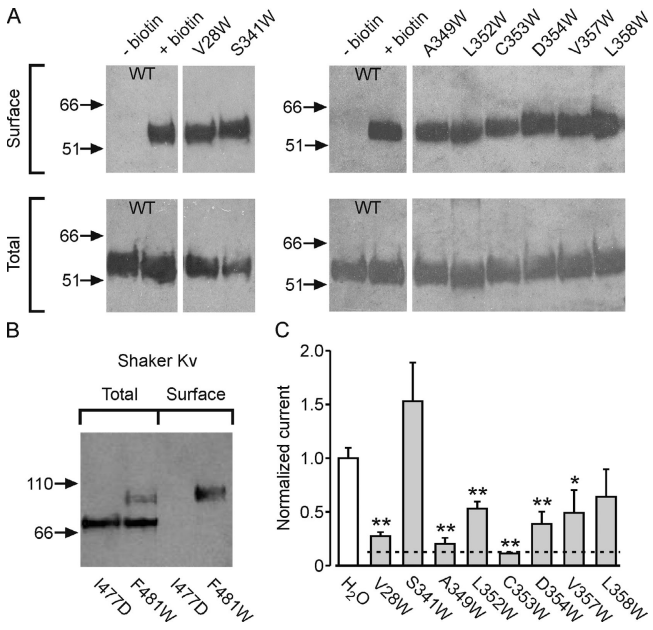

FIGURE 7. All of the nonfunctional mutants form nonconducting channels. (A) Western blots from SDS-PAGE of $P2X_4$ receptor channels obtained from surface membrane preparation (top) and total crude membrane preparation (bottom). Each lane contains the protein from an equivalent of 20 oocytes (surface) or 1 oocyte (total). All the oocytes expressing mutant channels were treated with biotin. The four left lanes and the eight right lanes are from two separate experiments. Numbers to the left are molecular weight markers in kD. (B) Western blots from SDS-PAGE of c-myc–tagged *Shaker* I477D and F481W protein obtained from surface membrane preparation (right two lanes) and total crude membrane preparation (left two lanes). Each lane contains the protein from an equivalent of 20 oocytes (surface) or 1 oocyte (total). F481W protein has two dominant forms, a core-glycosylated form (~70 kD) and a mature form (~100 kD). I477D exhibits only the core-glycosylated form. Numbers to the left are molecular weight markers in kD. (C) Mean ± SEM currents (averaged from 10 oocytes) from oocytes coinjected with 1:1 mixtures of cRNA for the WT and nonconducting mutant channel subunits. Oocytes injected with a 1:1 dilution of WT cRNA served as a control. The dashed line represents the expected current if the subunits randomly assemble to form trimers and a single mutant subunit prevents channel function. Significant differences between the control and each of the other groups was assessed with ungrouped Student's *t* test. *, $P < 0.05$; **, $P < 0.001$.

tional mutants in Kv channels, where nonfunctional mutants are often retained in the ER (Papazian et al., 1995; Tiwari-Woodruff et al., 1997; Hackos et al., 2002; Kitaguchi et al., 2004).

Coassembly of WT and Nonconducting Mutant Subunits

The surface expression of the nonfunctional mutant channels indicates that the mutations interfere with channel function and not with the maturation or trafficking of the protein. Thus, these results identify the inner part of TM2 as serving a critical functional role in either the processes of gating or ion conduction in $P2X_4$ receptor channels. To further substantiate this conclusion and to examine the dominance of mutant subunits in causing this nonconducting phenotype, we tested whether mutant and WT subunits could coassemble to form functional channels. Oocytes were coinjected with 1:1 mixtures of cRNA for the WT and nonconducting mutant channel subunits, and the current in response to 10 μM ATP was measured (Fig. 7 C). Oocytes injected with a 1:1 dilution of WT cRNA served as a control. If the mutant and WT subunits do not interact, then the expression level and conduction properties of the functional channels should be the same in oocytes injected with WT alone when compared with oocytes coinjected with mutant cRNA. At the other extreme, if WT and mutant subunits can randomly coassemble as trimers and a single mutant subunit is sufficient to silence the channel, then the current should be attenuated by 87.5% relative to the control (dashed line in Fig. 7 C). Current levels that do not fall into these two categories are more complicated to interpret, since coassembled channels might have altered unitary conductance and/or open probability in accordance with the number of mutant subunits per channel. Nevertheless, reduced or enhanced currents indicate coassembly if the differences from WT are statistically significant. Six of the nonconducting mutants (V28W, A349W, L352W, C353W, D354W, and V357W) significantly attenuated the current by 50–89%, suggesting that these mutant subunits coassemble with WT subunits. In three of these instances, the current was inhibited by an amount close to 87.5%, suggesting that these mutants may exhibit a dominant-negative phenotype, with a single copy of the mutation disrupting channel function.

DISCUSSION

In the present study, we investigated the secondary structure and movements of the TMs in rat $P2X_4$ receptor channels using tryptophan scanning mutagenesis, estimating changes in ATP sensitivity as a gauge for whether the substitution is well tolerated. A number of previous studies on rat $P2X_2$ receptor channels were undertaken to determine whether TM1 and TM2 line the pore, to locate the regions forming the gate, and to identify residues that account for the selectivity of the channel (Rassendren et al., 1997; Egan et al., 1998; Nakazawa et al., 1998a; Khakh et al., 1999; Virginio et al., 1999; Haines et al., 2001a,b; Jiang et al., 2001; Migita et al., 2001; Egan and Khakh, 2004). In addition, an alanine scanning mutagenesis study on the two TMs of the rat $P2X_2$ receptor channel was published while this manuscript was in preparation (Li et al., 2004). In the following we discuss the implications of the present results for the structure and gating of P2X receptor channels, referring to these earlier findings where pertinent.

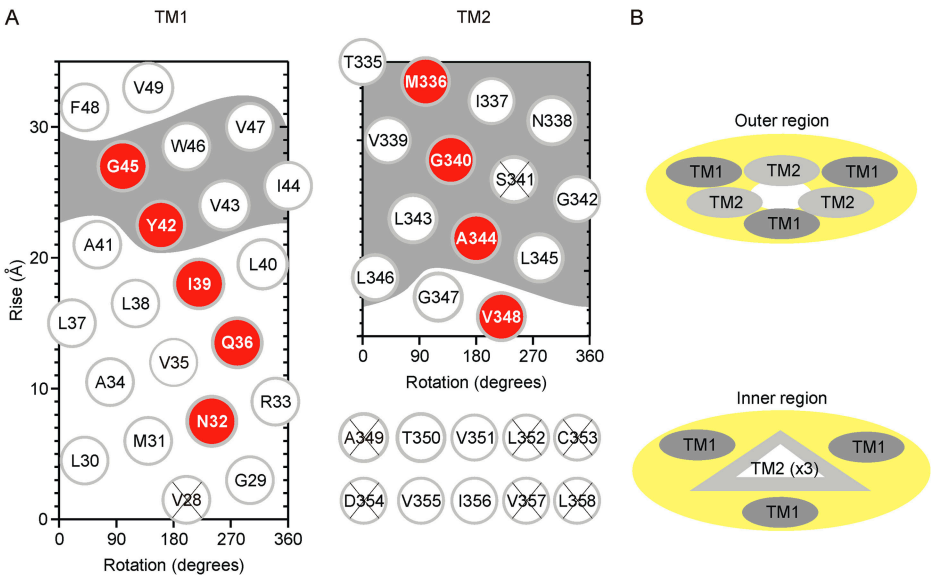

FIGURE 8. Proposed secondary structure and packing of the TMs of $P2X_4$ receptor channels. (A) TM1 and the outer region of TM2 are depicted as α-helical structures. The residues that exhibit the greatest perturbations in EC_{50} relative to the neighboring residues are in red. The regions of large perturbation in EC_{50} are shaded gray. Mutations that result in nonconducting channels are crossed out. (B) A schematic representation of the proposed packing of the TMs in the outer and inner regions of the membrane. Toward the inside, TM1 is depicted as being more peripheral, interacting with TM2 through the residues labeled in A in red. The inner triangle denotes that the secondary structural for the inner region of TM2 is undefined. Toward the outside, both TM1 and TM2 are depicted as α-helices, and are likely more tightly packed.

Secondary Structure of the TMs

The tryptophan scan of TM1 shows a clear pattern in ATP sensitivity (Figs. 3 and 4). Five residues, spanning the majority of TM1, are more sensitive to ATP than the neighboring residues, and all these residues map to one face of an α-helix. A helical secondary structure for TM1 is also supported by Fourier transform analysis (Fig. 4 C). A pattern consistent with helical structure was also seen for the outer half of TM2 (Figs. 5 and 6), however, Fourier transform analysis was not informative for this TM given the large number of nonconducting mutations. From these results, we conclude that the entire length of TM1 and probably at least the outer part of TM2 are α-helices, as depicted in Fig. 8 A where the residues on the sensitive face of the helices are indicated in red. The assignment of helical secondary structure from scanning mutagenesis studies has been validated by X-ray or atomic resolution EM structures in at least three instances, including inward rectifier K^+ channels (Choe et al., 1995; Cukras et al., 2002), voltage-activated K^+ channels (Monks et al., 1999; Hong and Miller, 2000; Li-Smerin et al., 2000a; Li-Smerin and Swartz, 2001; Jiang et al., 2003b), and nicotinic ACh receptor channels (Guzman et al., 2003; Miyazawa et al., 2003). An α-helical structure for TM1 has also been proposed in a recent alanine scanning mutagenesis study on the TMs of the $P2X_2$ receptor channel (Li et al., 2004). It is reassuring to note that all the positions in TM1 labeled in red in Fig. 8 A, except for G45, were also sensitive to alanine substitution in $P2X_2$. The alanine scan did not reveal an interpretable pattern for any part of TM2, possibly due to the more conservative nature of the alanine substitution for many positions in TM2. We have also made a number of alanine substitutions in TM2 and find that these mutants typically display a less severe phenotype than for tryptophan substitutions (unpublished data).

Why Do Tryptophan Substitutions Disproportionately Increase ATP Sensitivity?

One of the striking observations in the present study is that tryptophan substitutions most commonly increase the ATP sensitivity of the $P2X_4$ receptor channel (Figs. 3 and 5; Tables I and II). Whereas only 1 out of 38 mutations that give rise to functional ATP-activated channels (L40W) causes a decrease in ATP sensitivity of at least twofold, six mutations display more than a 10-fold increase in sensitivity to ATP (Tables I and II). A total of 20 mutations increase the sensitivity to ATP at least fourfold, while only two mutations display a reduced sensitivity to ATP. Because it is unlikely that mutations in TM1 and TM2 directly contribute to the ATP binding site (Nakazawa et al., 1998b; Ennion et al., 2000; Jiang et al., 2000; Roberts and Evans, 2004), we propose that these high-impact mutations increase the sensitivity to ATP by altering the closed–open equilibrium of the channel in favor of the open state. An introduced tryptophan could exert this effect on the closed–open equilibrium by either stabilizing the open state or destabilizing the closed state. It is improbable that introduction of tryptophan at so many positions would stabilize any particular conformation because this would require an improvement or optimization in packing. Thus, we favor the view that the large perturbations

in EC_{50} arise predominantly from destabilization of the closed conformation. Single channel experiments might be able to resolve this issue. However, $P2X_4$ receptor channels are difficult to study on the single channel level. These channels have a small conductance (12 pS at −150 mV), desensitize, and rapidly rundown in excised patches of membrane (Priel and Silberberg, 2004).

A disproportionate disruption of the closed conformation can be rationalized by proposing that the closed conformation of the transmembrane region of the channel is intrinsically more stable than the open conformation, and thus more readily perturbed by mutation. This idea has support from both structural and functional investigations on the transmembrane gate regions in K^+ channels. Inspection of the X-ray structures of KcsA, which is thought to be closed, and MthK, which is thought to be open, gives the impression that KcsA is a more optimally packed structure than MthK (Doyle et al., 1998; Jiang et al., 2002a,b). From functional studies, mutations in the gate region of the Shaker Kv channel also most commonly shift the closed–open equilibrium toward the open state (Hackos et al., 2002; Yifrach and MacKinnon, 2002), consistent with the notion that the closed gate is more stable. Thus, the type of perturbation observed here in $P2X_4$ is very consistent with an effect on the closed–open equilibrium, and with a more stable closed conformation of the transmembrane domain of the channel.

Arrangement of TMs around the Ion Conduction Pore

The ion conduction pore in P2X receptor channels is likely to be positioned at the central axis of the protein given that they have only two TMs per subunit and most likely assemble as trimers (Nicke et al., 1998; Stoop et al., 1999; Jiang et al., 2003a; Aschrafi et al., 2004), which provides too few helices to form more than one pore (Spencer and Rees, 2002). Two aspects of the present results are consistent with an arrangement of the TMs around the pore in which TM1 is more peripheral than TM2, as depicted in Fig. 8 B. First, there is a marked disparity between the two TMs in the number of mutations that give rise to nonconducting channels; TM1 contains one such mutant, whereas TM2 contains seven. Although we do not understand the underlying mechanism for the nonconducting mutants, the rather drastic nature of this phenotype suggests that these residues are likely to be buried in the protein. Second, the residues that tolerate mutation to tryptophan with only minor effects on the gating equilibrium are good candidates for positions that are exposed to the surrounding lipid. For TM1, 10 out of 22 mutations result in a less than twofold change in EC_{50}, whereas only 5 out of 24 mutations have similar weak effects in TM2.

The present results also suggest that the arrangement of the TMs around the pore is somewhat different for the outer and inner parts of the channel. In TM1, most of the tolerant positions are located in the inner half of the TM (below I39), suggesting that there is extensive lipid exposure in this region. The high impact residues in TM1 (Fig. 8 A) identify a face of the helix that is likely to be involved in protein–protein interactions that stabilize the closed conformation of the channel. Toward the outside of TM1 there is a stretch of six residues that show large changes in EC_{50} (shaded area in Fig. 8 A), suggesting that interactions between TM1 and other parts of the protein are more extensive in the outer region. This is portrayed as a more tightly packed arrangement of the TMs in the outer region relative to the inner region (Fig. 8 B), but could well involve interactions with other parts of the protein within the TM1–TM2 linker. In addition, the clustering of nonconducting mutants toward the inner part of TM2 also raises the possibility that the secondary structure is different for the inner and outer regions.

Where Is the Gate Region in P2X Receptor Channels?

The gate in an ion channel can be operationally defined as the region of the protein that serves to minimize the flow of ions in the closed conformation. In potassium channels, for example, the transmembrane helices form a physically occluding barrier to the movement of ions at the inner end of the pore (del Camino and Yellen, 2001; Armstrong, 2003). Opening of the gate in these channels is thought to involve movement of the transmembrane helices, although the nature and extent of the movements remains unresolved (Jiang et al., 2002b; Swartz, 2004; Webster et al., 2004). In the present study, the effects of tryptophan substitution on the closed–open equilibrium indicate that the local environment of the mutated residue is different in the open and closed states. Thus, the perturbations observed here strongly imply that the TMs move with channel opening. The distribution of perturbed positions throughout the TMs gives the impression of rather extensive rearrangements of the TMs during gating, rather than being restricted to a focal region. The clear bias for large perturbations toward the outer half of TM1 and TM2 (Y42-V47 and T335-L346; shaded areas in Fig. 8) indicates that these regions undergo significant environmental changes between open and closed states, although large perturbations do not necessarily indicate that the movements are correspondingly large. The notion of gating motions in the outer regions of the transmembrane domain is consistent with studies examining the differential sensitivity of $P2X_1$ and $P2X_2$ receptor channels to the partial agonist αβmeATP (Haines et al., 2001a) and with state dependence for MTS reaction (Jiang et al., 2001). One

possibility is that the gate resides in this outer region where we observed the type or perturbations expected for the tightly packed region that forms the barrier to ion conduction. In this regard it is interesting that two mutations in this region of the $P2X_2$ receptor channel (Y43A and F44A) have been recently proposed to result in conducting channels in the absence of agonist. Li et al. (2004) found that these mutations increase leak currents and promote cell death in HEK293 cells in the absence of ATP and in the presence of apyrase, an enzyme that catalyzes the hydrolysis of ATP. We have also found a similar phenomenon in $P2X_4$ for the Y42A mutation, which corresponds to Y43A in $P2X_2$. Oocytes injected with Y42A cRNA have reduced membrane potentials and a larger standing current at −80 mV when compared with oocytes expressing the WT receptor channel, and die within 2–3 d. As with the mutations in $P2X_2$ receptor channels, apyrase (10 U/ml) does not prevent the demise of the oocytes. There are two possible explanations for this phenomenon, both which support the notion that this region contributes to forming the gate. The Y42A mutation, which decreases side chain volume, might increase the flow of ions in the closed conformation, rendering the gate leaky, or the mutation may dramatically destabilize the closed conformation of the gate to increase the open probability in the absence of agonist (Soler-Llavina et al., 2003; Sukhareva et al., 2003). In K^+ channels, the mutations that result in constitutive activation are limited to the established gate region of the channel (Yi et al., 2001; Sukhareva et al., 2003), supporting the notion of a gate in the external region of the pore in P2X receptor channels.

A number of studies examining the accessibility of MTS reagents and Ag^+ to introduced Cys residues are also consistent with a gate in the outer regions of the transmembrane domain of P2X receptor channels. MTS accessibility experiments on TM2 of the rat $P2X_2$ receptor channel led Rassendren et al. (1997) to propose that the gate is in the middle of TM2 between L338 and D349 (L343 and D354 in $P2X_4$). Egan et al. (1998) suggested that TM2 is oriented such that L334, L338, and T339 (V339, L343, and A344 in $P2X_4$) are below the gate while G342 (G347 in $P2X_4$) is part of the gate since this residue was modified from both sides of the membrane by MTSEA. V48C in the rat $P2X_2$ receptor channel (V47 in $P2X_4$) is modified by MTS reagents more rapidly when the channel is activated by ATP than in its absence, suggesting movements in this region during gating (Jiang et al., 2001).

A Critical Inner Region

The present results also draw attention to the inner regions of the transmembrane domain of the channel, where seven nonconducting mutants are located, six of which are clustered within the inner part of TM2. The sensitivity of this inner region may reflect a tightly packed and relatively delicate structure that poorly tolerates substitution. However, it is worth keeping in mind that none of these mutants are ER retained, arguing against gross alterations in the protein fold. Most of the nonconducting mutants remain competent to coassemble with WT subunits, also arguing against a general disruption of oligomerization. It is tempting to speculate that this inner region of TM2 has an important role in either the gating or ion selectivity of P2X receptor channels. Although the results discussed above point to movements in the outer regions of the TMs, they do not exclude the involvement of the sensitive inner region in gating. In much the same way, the previous studies implicating outer regions of TM2 in ion conduction and selectivity (Nakazawa et al., 1998a; Migita et al., 2001; Egan and Khakh, 2004) do not rule out an important contribution of the inner region.

Conclusions

The results presented here provide evidence that TM1 and the outer region of TM2 adopt α-helical secondary structures in P2X receptor channels. The majority of mutations within the transmembrane domain enhance the sensitivity of the channel for ATP, suggesting that the closed conformation is more optimally packed. The distribution of perturbations in the closed–open equilibrium indicates that the outer regions of both TMs undergo rearrangements during gating. Finally, the distribution of mutations giving rise to nonconducting channels identifies an inner region of TM2 that may play a critical role in channel function.

We thank Florentina Soto and Walter Stühmer (Max-Planck-Institut fur Experimentelle Medizin, Gottingen, Germany) for providing the rat $P2X_4$ receptor channel DNA. Thanks to Miguel Holmgren, Tetsuya Kitaguchi and Joe Mindell for helpful discussions.

S. Silberberg was supported by the Sabbatical Program within the Intramural Research Program in the National Institutes of Neurological Disorders and Stroke.

Olaf S. Andersen served as editor.

Submitted: 19 November 2004
Accepted: 2 March 2005

REFERENCES

Armstrong, C.M. 2003. Voltage-gated K channels. *Sci STKE.* 2003: re10.

Aschrafi, A., S. Sadtler, C. Niculescu, J. Rettinger, and G. Schmalzing. 2004. Trimeric architecture of homomeric P2X2 and heteromeric P2X1+2 receptor subtypes. *J. Mol. Biol.* 342:333–343.

Brake, A.J., M.J. Wagenbach, and D. Julius. 1994. New structural motif for ligand-gated ion channels defined by an ionotropic ATP receptor. *Nature.* 371:519–523.

Chang, G., R.H. Spencer, A.T. Lee, M.T. Barclay, and D.C. Rees. 1998. Structure of the MscL homolog from Mycobacterium tuberculosis: a gated mechanosensitive ion channel. *Science.* 282:

2220–2226.

Choe, S., C.F. Stevens, and J.M. Sullivan. 1995. Three distinct structural environments of a transmembrane domain in the inwardly rectifying potassium channel ROMK1 defined by perturbation. *Proc. Natl. Acad. Sci. USA*. 92:12046–12049.

Collins, A., H. Chuang, Y.N. Jan, and L.Y. Jan. 1997. Scanning mutagenesis of the putative transmembrane segments of Kir2.1, an inward rectifier potassium channel. *Proc. Natl. Acad. Sci. USA*. 94: 5456–5460.

Cornette, J.L., K.B. Cease, H. Margalit, J.L. Spouge, J.A. Berzofsky, and C. DeLisi. 1987. Hydrophobicity scales and computational techniques for detecting amphipathic structures in proteins. *J. Mol. Biol.* 195:659–685.

Cukras, C.A., I. Jeliazkova, and C.G. Nichols. 2002. Structural and functional determinants of conserved lipid interaction domains of inward rectifying Kir6.2 channels. *J. Gen. Physiol.* 119:581–591.

del Camino, D., and G. Yellen. 2001. Tight steric closure at the intracellular activation gate of a voltage-gated K^+ channel. *Neuron.* 32:649–656.

Doyle, D.A., J. Morais Cabral, R.A. Pfuetzner, A. Kuo, J.M. Gulbis, S.L. Cohen, B.T. Chait, and R. MacKinnon. 1998. The structure of the potassium channel: molecular basis of K^+ conduction and selectivity. *Science.* 280:69–77.

Dutzler, R., E.B. Campbell, M. Cadene, B.T. Chait, and R. MacKinnon. 2002. X-ray structure of a ClC chloride channel at 3.0 A reveals the molecular basis of anion selectivity. *Nature.* 415:287–294.

Egan, T.M., W.R. Haines, and M.M. Voigt. 1998. A domain contributing to the ion channel of ATP-gated P2X2 receptors identified by the substituted cysteine accessibility method. *J. Neurosci.* 18: 2350–2359.

Egan, T.M., and B.S. Khakh. 2004. Contribution of calcium ions to P2X channel responses. *J. Neurosci.* 24:3413–3420.

Ennion, S., S. Hagan, and R.J. Evans. 2000. The role of positively charged amino acids in ATP recognition by human P2X(1) receptors. *J. Biol. Chem.* 275:29361–29367.

Ennion, S.J., and R.J. Evans. 2002. Conserved cysteine residues in the extracellular loop of the human P2X(1) receptor form disulfide bonds and are involved in receptor trafficking to the cell surface. *Mol. Pharmacol.* 61:303–311.

Guzman, G.R., J. Santiago, A. Ricardo, R. Marti-Arbona, L.V. Rojas, and J.A. Lasalde-Dominicci. 2003. Tryptophan scanning mutagenesis in the αM3 transmembrane domain of the *Torpedo californica* acetylcholine receptor: functional and structural implications. *Biochemistry.* 42:12243–12250.

Hackos, D.H., T.H. Chang, and K.J. Swartz. 2002. Scanning the intracellular S6 activation gate in the shaker K^+ channel. *J. Gen. Physiol.* 119:521–532.

Haines, W.R., K. Migita, J.A. Cox, T.M. Egan, and M.M. Voigt. 2001a. The first transmembrane domain of the P2X receptor subunit participates in the agonist-induced gating of the channel. *J. Biol. Chem.* 276:32793–32798.

Haines, W.R., M.M. Voigt, K. Migita, G.E. Torres, and T.M. Egan. 2001b. On the contribution of the first transmembrane domain to whole-cell current through an ATP-gated ionotropic P2X receptor. *J. Neurosci.* 21:5885–5892.

Hong, K.H., and C. Miller. 2000. The lipid-protein interface of a Shaker K^+ channel. *J. Gen. Physiol.* 115:51–58.

Jenkins, A., A. Andreasen, J.R. Trudell, and N.L. Harrison. 2002. Tryptophan scanning mutagenesis in TM4 of the GABA(A) receptor α1 subunit: implications for modulation by inhaled anesthetics and ion channel structure. *Neuropharmacology.* 43:669–678.

Jiang, L.H., M. Kim, V. Spelta, X. Bo, A. Surprenant, and R.A. North. 2003a. Subunit arrangement in P2X receptors. *J. Neurosci.* 23:8903–8910.

Jiang, L.H., F. Rassendren, V. Spelta, A. Surprenant, and R.A. North. 2001. Amino acid residues involved in gating identified in the first membrane-spanning domain of the rat P2X(2) receptor. *J. Biol. Chem.* 276:14902–14908.

Jiang, L.H., F. Rassendren, A. Surprenant, and R.A. North. 2000. Identification of amino acid residues contributing to the ATP-binding site of a purinergic P2X receptor. *J. Biol. Chem.* 275: 34190–34196.

Jiang, Y., A. Lee, J. Chen, M. Cadene, B.T. Chait, and R. MacKinnon. 2002a. Crystal structure and mechanism of a calcium-gated potassium channel. *Nature.* 417:515–522.

Jiang, Y., A. Lee, J. Chen, M. Cadene, B.T. Chait, and R. MacKinnon. 2002b. The open pore conformation of potassium channels. *Nature.* 417:523–526.

Jiang, Y., A. Lee, J. Chen, V. Ruta, M. Cadene, B.T. Chait, and R. MacKinnon. 2003b. X-ray structure of a voltage-dependent K^+ channel. *Nature.* 423:33–41.

Khakh, B.S., X.R. Bao, C. Labarca, and H.A. Lester. 1999. Neuronal P2X transmitter-gated cation channels change their ion selectivity in seconds. *Nat. Neurosci.* 2:322–330.

Kitaguchi, T., M. Sukhareva, and K.J. Swartz. 2004. Stabilizing the closed S6 gate in the Shaker Kv channel through modification of a hydrophobic seal. *J. Gen. Physiol.* 124:319–332.

Komiya, H., T.O. Yeates, D.C. Rees, J.P. Allen, and G. Feher. 1988. Structure of the reaction center from *Rhodobacter sphaeroides* R-26 and 2.4.1: symmetry relations and sequence comparisons between different species. *Proc. Natl. Acad. Sci. USA*. 85:9012–9016.

Kuo, A., J.M. Gulbis, J.F. Antcliff, T. Rahman, E.D. Lowe, J. Zimmer, J. Cuthbertson, F.M. Ashcroft, T. Ezaki, and D.A. Doyle. 2003. Crystal structure of the potassium channel KirBac1.1 in the closed state. *Science.* 300:1922–1926.

Lester, H.A., M.I. Dibas, D.S. Dahan, J.F. Leite, and D.A. Dougherty. 2004. Cys-loop receptors: new twists and turns. *Trends Neurosci.* 27:329–336.

Li, Z., K. Migita, D.S. Samways, M.M. Voigt, and T.M. Egan. 2004. Gain and loss of channel function by alanine substitutions in the transmembrane segments of the rat ATP-gated P2X2 receptor. *J. Neurosci.* 24:7378–7386.

Liman, E.R., J. Tytgat, and P. Hess. 1992. Subunit stoichiometry of a mammalian K^+ channel determined by construction of multimeric cDNAs. *Neuron.* 9:861–871.

Li-Smerin, Y., D.H. Hackos, and K.J. Swartz. 2000a. α-Helical structural elements within the voltage-sensing domains of a K^+ channel. *J. Gen. Physiol.* 115:33–50.

Li-Smerin, Y., D.H. Hackos, and K.J. Swartz. 2000b. A localized interaction surface for voltage-sensing domains on the pore domain of a K^+ channel. *Neuron.* 25:411–423.

Li-Smerin, Y., and K.J. Swartz. 2001. Helical structure of the COOH terminus of S3 and its contribution to the gating modifier toxin receptor in voltage-gated ion channels. *J. Gen. Physiol.* 117:205–218.

Migita, K., W.R. Haines, M.M. Voigt, and T.M. Egan. 2001. Polar residues of the second transmembrane domain influence cation permeability of the ATP-gated P2X(2) receptor. *J. Biol. Chem.* 276:30934–30941.

Miyazawa, A., Y. Fujiyoshi, and N. Unwin. 2003. Structure and gating mechanism of the acetylcholine receptor pore. *Nature.* 423: 949–955.

Monks, S.A., D.J. Needleman, and C. Miller. 1999. Helical structure and packing orientation of the S2 segment in the Shaker K^+ channel. *J. Gen. Physiol.* 113:415–423.

Nakazawa, K., K. Inoue, and Y. Ohno. 1998a. An asparagine residue regulating conductance through P2X2 receptor/channels. *Eur. J. Pharmacol.* 347:141–144.

Nakazawa, K., Y. Ohno, and K. Inoue. 1998b. An aspartic acid resi-

due near the second transmembrane segment of ATP receptor/channel regulates agonist sensitivity. *Biochem. Biophys. Res. Commun.* 244:599–603.

Newbolt, A., R. Stoop, C. Virginio, A. Surprenant, R.A. North, G. Buell, and F. Rassendren. 1998. Membrane topology of an ATP-gated ion channel (P2X receptor). *J. Biol. Chem.* 273:15177–15182.

Nicke, A., H.G. Baumert, J. Rettinger, A. Eichele, G. Lambrecht, E. Mutschler, and G. Schmalzing. 1998. P2X1 and P2X3 receptors form stable trimers: a novel structural motif of ligand-gated ion channels. *EMBO J.* 17:3016–3028.

North, R.A. 2002. Molecular physiology of P2X receptors. *Physiol. Rev.* 82:1013–1067.

Panchenko, V.A., C.R. Glasser, and M.L. Mayer. 2001. Structural similarities between glutamate receptor channels and K^+ channels examined by scanning mutagenesis. *J. Gen. Physiol.* 117:345–360.

Papazian, D.M., X.M. Shao, S.A. Seoh, A.F. Mock, Y. Huang, and D.H. Wainstock. 1995. Electrostatic interactions of S4 voltage sensor in Shaker K^+ channel. *Neuron.* 14:1293–1301.

Priel, A., and S.D. Silberberg. 2004. Mechanism of ivermectin facilitation of human P2X4 receptor channels. *J. Gen. Physiol.* 123: 281–293.

Rassendren, F., G. Buell, A. Newbolt, R.A. North, and A. Surprenant. 1997. Identification of amino acid residues contributing to the pore of a P2X receptor. *EMBO J.* 16:3446–3454.

Rees, D.C., L. DeAntonio, and D. Eisenberg. 1989a. Hydrophobic organization of membrane proteins. *Science.* 245:510–513.

Rees, D.C., H. Komiya, T.O. Yeates, J.P. Allen, and G. Feher. 1989b. The bacterial photosynthetic reaction center as a model for membrane proteins. *Annu. Rev. Biochem.* 58:607–633.

Roberts, J.A., and R.J. Evans. 2004. ATP binding at human P2X1 receptors. Contribution of aromatic and basic amino acids revealed using mutagenesis and partial agonists. *J. Biol. Chem.* 279: 9043–9055.

Silberberg, S.D., and K.J. Swartz. 2004. Probing the structure of P2X receptor channels with ivermectin. *Biophys. J.* 86:356a.

Soler-Llavina, G.J., M. Holmgren, and K.J. Swartz. 2003. Defining the conductance of the closed state in a voltage-gated K^+ channel. *Neuron.* 38:61–67.

Spencer, R.H., and D.C. Rees. 2002. The alpha-helix and the organization and gating of channels. *Annu. Rev. Biophys. Biomol. Struct.* 31:207–233.

Stoop, R., S. Thomas, F. Rassendren, E. Kawashima, G. Buell, A. Surprenant, and R.A. North. 1999. Contribution of individual subunits to the multimeric P2X(2) receptor: estimates based on methanethiosulfonate block at T336C. *Mol. Pharmacol.* 56:973–981.

Sukhareva, M., D.H. Hackos, and K.J. Swartz. 2003. Constitutive activation of the Shaker Kv channel. *J. Gen. Physiol.* 122:541–556.

Swartz, K.J. 2004. Opening the gate in potassium channels. *Nat. Struct. Mol. Biol.* 11:499–501.

Tamamizu, S., G.R. Guzman, J. Santiago, L.V. Rojas, M.G. McNamee, and J.A. Lasalde-Dominicci. 2000. Functional effects of periodic tryptophan substitutions in the αM4 transmembrane domain of the *Torpedo californica* nicotinic acetylcholine receptor. *Biochemistry.* 39:4666–4673.

Tiwari-Woodruff, S.K., C.T. Schulteis, A.F. Mock, and D.M. Papazian. 1997. Electrostatic interactions between transmembrane segments mediate folding of Shaker K^+ channel subunits. *Biophys. J.* 72:1489–1500.

Valera, S., N. Hussy, R.J. Evans, N. Adami, R.A. North, A. Surprenant, and G. Buell. 1994. A new class of ligand-gated ion channel defined by P2x receptor for extracellular ATP. *Nature.* 371:516–519.

Virginio, C., A. MacKenzie, F.A. Rassendren, R.A. North, and A. Surprenant. 1999. Pore dilation of neuronal P2X receptor channels. *Nat. Neurosci.* 2:315–321.

Walz, T., T. Hirai, K. Murata, J.B. Heymann, K. Mitsuoka, Y. Fujiyoshi, B.L. Smith, P. Agre, and A. Engel. 1997. The three-dimensional structure of aquaporin-1. *Nature.* 387:624–627.

Webster, S.M., D. Del Camino, J.P. Dekker, and G. Yellen. 2004. Intracellular gate opening in Shaker K^+ channels defined by high-affinity metal bridges. *Nature.* 428:864–868.

Wollmuth, L.P., and A.I. Sobolevsky. 2004. Structure and gating of the glutamate receptor ion channel. *Trends Neurosci.* 27:321–328.

Yi, B.A., Y.F. Lin, Y.N. Jan, and L.Y. Jan. 2001. Yeast screen for constitutively active mutant G protein-activated potassium channels. *Neuron.* 29:657–667.

Yifrach, O., and R. MacKinnon. 2002. Energetics of pore opening in a voltage-gated K^+ channel. *Cell.* 111:231–239.